Thermal image processing for real-time noncontact respiration rate monitoring

ALKALI, Abdulkadir, SAATCHI, Reza <http://orcid.org/0000-0002-2266-0187>, ELPHICK, Heather and BURKE, Derek

Published version

ALKALI, Abdulkadir, SAATCHI, Reza, ELPHICK, Heather and BURKE, Derek (2017). Thermal image processing for real-time noncontact respiration rate monitoring. IET Circuits, Devices and Systems, 11 (2), 142-148.

Thermal Image Processing for Real-Time Noncontact Respiration Rate Monitoring

Abdulkadir H Alkali[1], Reza Saatchi[1], Heather Elphick[2], Derek Burke[2]

[1]Department of Engineering and Mathematics, Sheffield Hallam University, Sheffield, United Kingdom
[2]Sheffield Children's Hospital National Health Service Trust, Sheffield, United Kingdom

Abstract

A real-time thermal imaging based, noncontact respiration rate monitoring method was developed. It measured the respiration related skin surface temperature changes under the tip of the nose. Facial tracking was required as head movements caused the face to appear in different locations in the recorded images over time. The algorithm detected the tip of the nose and then, a region just under it was selected. The pixel values in this region in successive images were processed to determine respiration rate. The segmentation method, used as part of the facial tracking, was evaluated on 55,000 thermal images recorded from 14 subjects with different extent of head movements. It separated the face from image background in all images. However, in 11.7% of the images, a section of the neck was also included, but this did not cause an error in determining respiration rate.

The method was further evaluated on 15 adults, against two contact respiration rate monitoring methods that tracked thoracic and abdominal movements. The three methods gave close respiration rates in 12 subjects but in 3 subjects, where there were very large head movements, the respiration rates did not match.

Keywords: Medical Image Processing, Medical Signal Processing, Medical Diagnostic Computing.

1 Introduction

Respiration is an important physiological process [1]. The average number of times air is inhaled and exhaled per minute is respiration rate. Respiration rate is an important discriminatory indicator of urgency for medical attention [2]. It needs accurate measurement in sleep related studies and disorders, neonatal care, critically ill patients and the diagnosis and management of respiratory diseases [3-5]. Respiration produces numerous detectable signs, e.g. chest and abdomen movements and variations in infrared emission from the skin surface centred on the tip of the nose [6]. Existing respiration rate monitors are generally contact based [7], i.e. they need to be attached to the subject's body, thus causing discomfort during recording [8], which in turn may alter respiration rate. The attached monitor can also become dislodged and body movements can interfere with their readings.

There were a number of studies to develop noncontact respiration rate monitors based on technologies such as video imaging, ultrasound and radar detection and air flow measurement [9-17]. Video monitoring tracks chest and abdominal movements. It however suffers from illumination variations and is not practical in low light intensity environments [14]. Ultrasound and radar based respiration rate monitors are highly sensitive to body movements.

Thermal imaging as a technology for long term respiration rate monitoring, has recently become more realistic as thermal imaging devices have significantly improved in their scanning speed, sensitivity and portability, while their cost has reduced [18]. They can accurately measure facial skin surface temperature changes under the tip of the nose as air is inhaled and exhaled and these are in turn processed to indicate respiration rate.

In this study, to search for the facial region most affected by respiration, the face was initially segmented from the image by modifying the construction of mosaic image algorithm reported in [19], and then the regions' boundaries were identified using the projections of the image using the method reported in [20]. The face was then tracked in successive images and the facial regions to monitor respiration rate were localised.

A number of methods were reported for detecting and tracking the facial features in thermal images for respiration rate monitoring. Mostafa *et al.* [21] reported a method that detected and tracked a facial region for respiration rate monitoring. It consisted of parts that detected the suitable regions and updates them. A method based on Haar-like features was proposed in [22], enhanced in [23] and was employed in [24] to detect the nasal cavity in thermal images. It relied on setting a predefined threshold for detecting the facial region that needed the temperature of the environment and the subjects to be constant. The facial tracking method reported in [25] filtered the thermal images, segmented the subject’s face from the image background and located the two warmest points on the face that corresponded to the inner corners of the eyes. Once these two points were located, the coolest facial region beneath them was located. This corresponded to the tip of the nose. A circle was then placed over this region and the pixel values within it were averaged to produce a point on the respiration signal. The method however did not operate in real-time due to high computational intensity.

Martinez *et al.* [26] detected the eyes and nostrils in thermal images by considering the image segments that had intensities similar to those of the skin temperature and extracted their features using the Haar wavelets. The method was computationally intensive.

In [27] a region beneath the tip of the nose was chosen as a respiration region of interest and was tracked using the method described in [28]. The subjects mostly made minor head movements and were in profile view of the camera. Coalitional tracking algorithm was reported in [29] to track the face and during the first image, a grid outline that composed of four particle filter trackers was manually selected over the nose. The left and right boundaries of the nose were detected by obtaining the horizontal gradients of the grid, while the locations of the nostrils were identified by examining the vertical and horizontal projection profiles of the nose.

A coalitional tracking was also reported in [30]. The coalitional tracking reported in [31] was based on a preselection of a template, thus requiring a user intervention. A solution to template pre-selection that could deal with the issues highlighted in [29-31] was reported in [32]. It however was constrained by several issues, e.g. computational intensity, need for selecting a suitable threshold, requirement for face to be stationary at the start and detection of an involuntary eye blink.

A particle filter tracker was used to update a manually selected template of a facial region [33]. The filter was based on a probabilistic template function and correlation analysis.

In thermal imaging, infrared radiation emitted from an object is dependent on its surface temperature and emissivity. Emissivity measures the amount of infrared radiation from an object as compared to a black body at the same temperature**.** For the human skin at 32 ^{o}C, the emissivity is about 0.98 [34]. The infrared spectrum has a wavelength ranging between 750 nm to $1\,\mathrm{mm}$ ($400\,\mathrm{THz}$ to $300\,\mathrm{GHz}$) range. Thermal imaging is unaffected by illumination and is a safe technology [35].

In this study, a real-time thermal imaging based respiration rate monitoring that detected facial skin surface temperature changes under the nose tip was developed and its performance was evaluated. The tracking method in this study reduces the restrictions on the subject during the recording as compared with the earlier studies thus providing a significant advance on noncontact real time respiration rate monitoring.

In the following sections, the methodology, results and conclusions of the study are explained.

2 Methodologies

2.1 Recruitment

Ethics approvals for the study were obtained from Sheffield Hallam University and the National Health Service (NHS), UK. An assessment of facial features detection method was carried out on 55,000 thermal images recorded from 14 adults at Sheffield Hallam University. A further evaluation in determining respiration rate was carried out against two contact based respiration rate monitoring methods. These operated by detecting thoracic and abdominal movements. This evaluation was performed on 15 adult volunteers (mean age 36.6 years, standard deviation 8.2 years) in a hospital setting after obtaining informed consent.

2.2 Experimental setup

A FLIR A40 thermal camera was used in this study. This has a field of view of 24^{o} x 18^{o} with a spectral range (i.e. the portion of electromagnetic spectrum detected by camera) of 7.5 µm to 13.0 µm, maximum 50 images per second capture rate, image size 320 x 240 pixels, temperature range -40 to 500 ºC and thermal sensitivity 0.08 Kelvin. The camera's emissivity was set to 0.98 as this is suitable for skin surface

temperature measurement. The camera was connected to a 32-bit laptop computer using IEEE 1398 (FireWire) communication protocol.

Thoracic and abdominal piezoelectric bands based respiration rate monitors were used to assess the performance of the thermal imaging method on the 15 subjects enrolled at the hospital. The thermal camera was mounted on a tripod, about 1 meter from where the subject sat comfortably on a chair. The subject's face and a section of each shoulder were visible in the camera's field of view. The mean temperature and relative humidity of the recording room were 24.4°C (standard deviation of 0.35) and 45% (standard deviation of 0.71) respectively. The ambient temperature and humidity did not have a significant effect on the reported results as they were broadly consistent during recordings and also the method measured the relative changes in the skin temperature and thus to an extent negated minor ambient changes.

The image capture rate was 10 per second and recording duration was at least 10 minutes per subject. The image capture rate was sufficiently high to measure respiration rate and allowed real time processing. The camera was controlled by software developed using the National Instrument's LabVIEW environment. A brief overview of the processes is provided in the following paragraph and more detailed explanations are included in the following sections.

The subject's face was first localised in each image as explained in Section 2.4. The detected facial area was then searched to locate the inner corners of the eyes and from it the nose (coolest facial region). A region of interest (ROI) was created under the tip of the nose and the pixel values within it were averaged to produce a single feature for each image. A respiration signal was produced by plotting the features

from successive images over time. Respiration rate was determined from this signal by obtaining its fast Fourier transform.

2.3 Image Processing tasks during the recording stage

A median filter was applied to the images to remove obscuring high frequencies. A copy of each image i_C was created (for use in later stages) and normalised from its original 16 bits to 8 bits to reduce memory requirement. The original images were segmented to remove objects with temperatures significantly lower than the skin temperature. Three algorithms were compared for this segmentation: inter-variance (Otsu method) [36], moment (Tsai method) [37] and entropy (Kapur *et al*. method) [38]. The procedure for choosing between these methods was reported in [6]. Briefly, this involved manually segmenting the image to produce the ground-truth by experimenting with different segmentation thresholds and visually observing the outcome against the subject in the image. The ground-truth was compared against the segmented images obtained using the inter-variance, moment and entropy. This was performed by determining the total number of pixels (P_{tg}) in the ground-truth that had a binary value of 1 and then ANDing these pixels with the segmented image using each of the three techniques. The total number of pixels (P_{tm}) in the resulting image that were 1 was determined. The closeness of each segmentation to the ground-truth was determined by

$$Percentage\ closeness = \frac{P_{tm}}{P_{tg}} \times 100 \quad (1)$$

The inter-variance method was used in this study as it was closest to the ground-truth. The algorithm's computational requirement was sufficiently low for real-time operation.

2.4 Face detection and tracking

In a study the mosaic of images were used for face detection in black and white images [19]. The mosaic reduced the resolution of the image by dividing it into square cells and replacing the intensity of pixels in each cell by their average. We have adapted this technique to perform face detection in thermal images. In our method, the mosaic image I_m was constructed by dividing the segmented image I_s into square cells of sides k pixels and setting the grey level pixels in each cell equal to the maximum grey level pixel within the cell in order to make the higher temperature regions such as the corners of the eyes more prominent. Different *k* values in the range of 2 to 32 were experimented and *k* = 8 was chosen as it gave a better localisation of the face.

The horizontal ($H_p(x)$) and vertical ($V_p(y)$) projections of the mosaic image were obtained for an $M \times N$ image (*I(x,y)*) as:

$$H_p(x) = \frac{1}{M}\sum_{x=0}^{M-1} I(x,y) \quad (2)$$

$$V_p(y) = \frac{1}{N}\sum_{y=0}^{N-1} I(x,y) \quad (3)$$

As only the subject remained in I_s, the projections gave zero values for all points, except where the subject was in the image. This helped in dealing with false abrupt positive changes that could be mistaken as the side of the face. A simpler approach, considering that only the subject remained in the image, would have been to discard the null points and consider the sides of the face. This would have been valid if only the subject's face was in the image, but since parts of the shoulders also appeared in the image, it was not valid. To improve the effectiveness of detecting the sides of the face, the points where there were abrupt incremental changes at both the vertical and horizontal projections were present were located. The coordinates of these points are marked as $(x_{lt,}y_{lt})$, (x_{rt}, y_{rt}), $(x_{lb,}y_{lb})$ as (x_{rb}, y_{rb}) as indicated in Figure 1.

The abrupt changes on both projections were present because the face had a higher temperature than other parts of the body appearing in the image.

2.5 Detecting the inner corners of the eyes

In order to detect the inner corners of the eyes a search region and an approach to analyse it were needed. These are explained in the next sections.

2.5.1 Determining the search region

In the horizontal profile ($H_p(x)$), a region existed between the detected sides that contained information about the location of the inner corners of the eyes (Figure 1b). This region exhibited largest abrupt changes, mainly because the inner corners of the eyes have highest segmented facial temperature. This temperature difference was further enhanced by the method in which the pixel values within each cell were replaced by their maximum. The local top and bottom minima on the horizontal profile, where these changes occurred were marked as top (x_{tf}) and bottom (x_{bf}) feature areas respectively. Since this information did not specify the vertical coordinates of the inner corners of the eyes, a search area was created spanning from the left y_{lt} to the right y_{rt} boundaries. Thus the feature search area F_{sa} was over a region that was contained within (x_{tf}, y_{lt}) to (x_{bf}, y_{rt}).

2.5.2 Search region analysis approach

According to the anthropometry of the face, the separation between the inner corners of the two eyes (i.e. the distance between the two medial inter-canthals, *B*) is approximately one-fifth of the breadth of the head (*H)* [39, 40]. Therefore, a search template of size $3\frac{H}{5}$ was created. The search was initiated from the left-top corner of the selected region, moving forward by a pixel at a time to the end of the right side and then returning the left, a pixel below the previous row. The template that contained two peaks, separated by about $\frac{H}{5}$, indicated the location of the inner

corners of the eyes. When the face was fully visible in the image, the template contained two peaks with similar magnitudes separated by about $\frac{H}{5}$. For images that full face was not visible, the side of the eye nearest to the camera had a larger peak.

2.6 Detection of the tip of the nose

The tip of the nose was located by the vertical projection of the region enclosed by the identified inner corners of the eyes and the bottom boundary of the face. As the tip of the nose is the coolest facial point under the eyes, it corresponded to the lowest point in this vertical projection (shown in Figure 3).

2.7 Generation of respiration signal

Once the tip of the noise was detected, a circle with radius 5 pixels was placed under it and pixel values within it were averaged to produce a point on the respiration signal. This process was repeated for the successive images and every 20 consecutive points of the respiration signal were filtered using a 4^{th}-order Butterworth filter that had a cut off frequency of 2 Hz. The respiration signal was continuously displayed in real-time to aid monitoring of the data recording. After each 1024 points, the filtered signal was windowed with the Kaiser window (flatness value = 0.5, this value was chosen as it suitably tapered the signal edges without significantly altering its shape) and its magnitude frequency spectrum was obtained. The frequency corresponding to the largest peak in the spectrum was multiplied by 60 to obtain respiration rate in cycles per minute.

3 Results and Discussion

In this section the study's results for segmenting the images to localise face, detecting the inner corners of the eyes, identifying the tip of the nose and generating the respiration signal are presented. The respiration rate values obtained using

thermal imaging are compared against the values obtained using the two contact respiration rate monitors.

3.1 Image segmentation to extract of subject's face

The segmentation results comparing the ground-truth, entropy, moment and inter-variance methods to extract the subject from the image background are summarised in Table 1. The accuracy of inter-variance method was highest, providing 99.9% closeness (determined using equation 1) to the ground truth.

Table 1 Segmentation performance comparison

Segmentation Method	% Closeness to the ground truth
Entropy	82.8
Moment	40.2
Inter-variance	99.9

Figures 1a and 1b show typical vertical and horizontal facial profiles. They indicate the average pixel temperature intensities against column number for Figure 1a and row number for Figure 1b. Figure 1c indicates the localised face enclosed by a rectangle as determined by the two profiles.

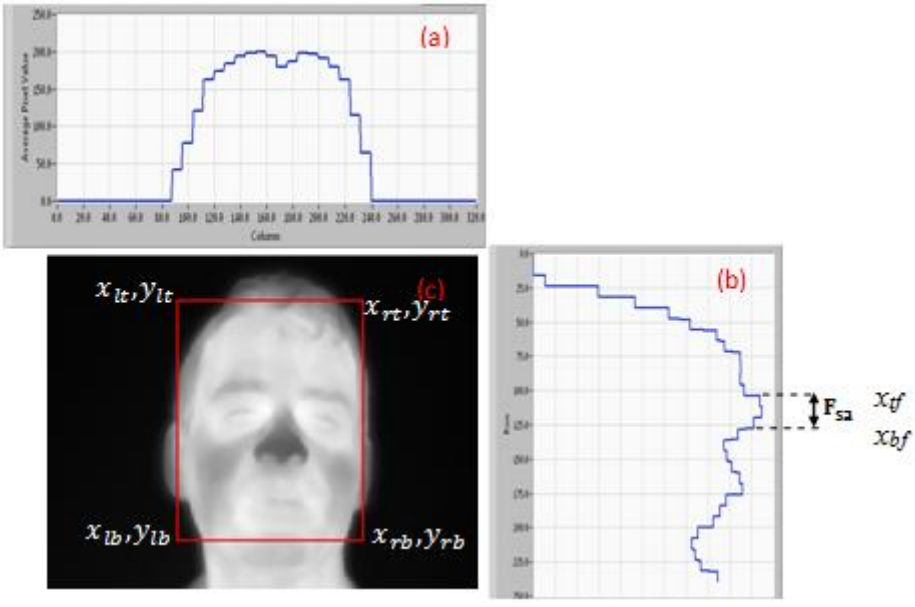

Figure 1 (a) vertical, (b) horizontal profiles and (c) localised face

The facial localisation method was evaluated 55000 thermal images recorded from 14 adult subjects. The images contained the head and a part of the shoulders. The method localised the face in all images, but in 11.7% of images, a section of the neck was also extracted. This assessment used the information from the anthropometry of the face in which the face length is expected to be more than 1.5 times its width [39, 40].

Figure 2 shows the search area (F_{sa}) to localise the inner corners of the eyes in three subjects. The area was detected from the horizontal profiles shown in Figure 1(b).

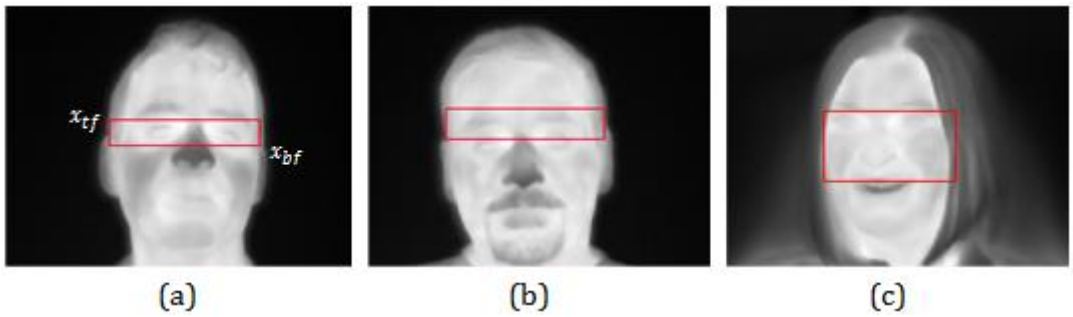

Figure 2 Search area to locate the inner corners of the eyes in three subjects.

The area contained the inner corners of the eyes and covered a region from the left side to the right side of the face. It was centred on the inner corners of the eyes (as shown in Figure 2a) in most subjects, however in few cases, the region moved slightly higher (as in the case in Figure 2b) or lower (as in the case in Figure 2c). The height of the rectangle containing the inner corners of the eyes depended on the temperature profile of the segmented face and thus varied in between subjects. Subjects (such as the one in Fig.2a) with cooler skin temperature within this region had a smaller search region than those with a warmer facial skin (e.g. Fig.2c). In all

cases the inner corners of the eyes were correctly identified due to the temperature dominance of the regions around the inner corners of the eyes.

Figures 3a and b show the vertical profile of F_{sa} and the localised corners of the eyes respectively. There are two dominant peaks in the profile with the plot bounded within F_{sa} and the locations of the two peaks matched the horizontal locations of the inner corners of the eyes.

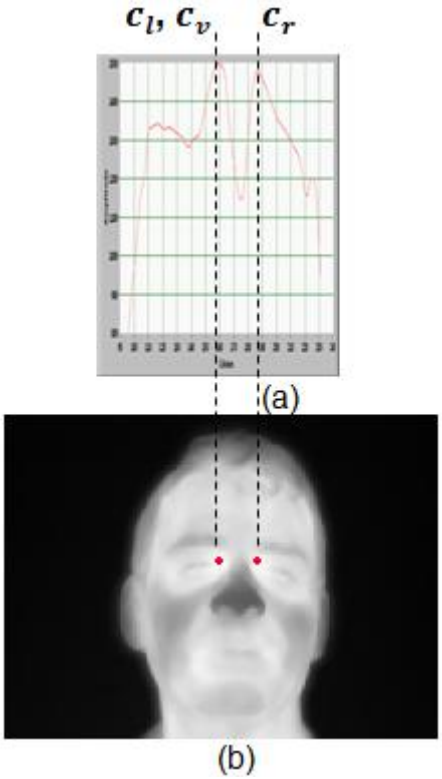

Figure 3 (a) The vertical profile of F_{sa} and (b) automatic identification the eyes' inner corners (shown as red dots).

The two peaks in the vertical profiles shown in Figure 3a do not have an identical magnitude as the head is slightly oriented to one side in relation to the camera. To investigate the robustness of detecting the inner corners of the eyes, the distance between the two detected inner corners of the eyes was determined. This distance was expected to be a quarter or less than a fifth of the width of the face [39, 40]. In 89.6% of 55000 images, the distance between the detected inner corners of the eyes

conformed to this expectation. In 10.4% of the images, the inner corners of the eyes were not the warmest facial points. This was caused by facial skin abnormalities such as scars.

A tip of the nose location search area that includes a region between the two corners of the eyes and bottom boundary of the detected face is shown in Figure 4a. The width and height of the rectangle enclosing the nose was set by the vertical and horizontal temperature distributions of pixels respectively (the details of the process are provided in section 2.5). The coolest point in this area was the tip of the nose. The identification of this point by the method is shown in Figure 4b.

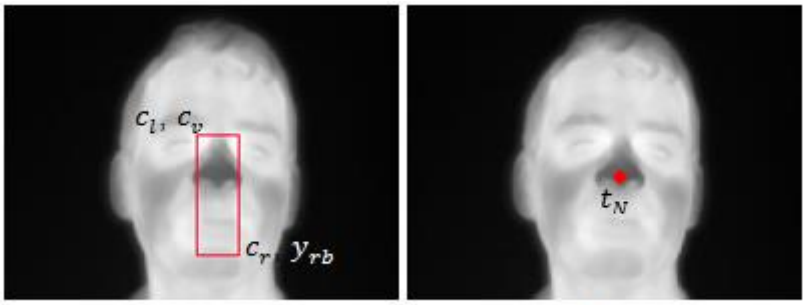

Figure 4 (a) nose search area, (b) identified tip of the nose indicated as t_N

Once the tip of the nose (t_N) was detected, a respiration region interest (ROI) was created beneath it. The skin surface in this region was sensitive to temperature changes caused by respiration. This region was represented by a circle, radius=5 pixels. The pixel values within it were averaged to produce a point for the respiration signal. A plot of these points from consecutive recorded images produced a respiration signal. The signal was compared with the respiration signals obtained from the ground truths which were obtained using thoracic and abdominal bands systems. The magnitude of the respiration signals from the ground truth methods was larger than the signal obtained using thermal imaging. Therefore, they were

scaled so that they could be shown on the same plots. Also, to facilitate comparison with the other signals, the signal from thermal imaging method was inverted as it was 180 degree out of phase with the ground truths.

3.2 Comparison of respiration signals and respiration rates obtained using the three methods

Figures 5 and 6 show typical respiration signals obtained using contact based ground truths and thermal imaging recorded from two subjects. The duration of the plot shown was restricted to 30 seconds of the 10 minutes recording to aid its visualisation.

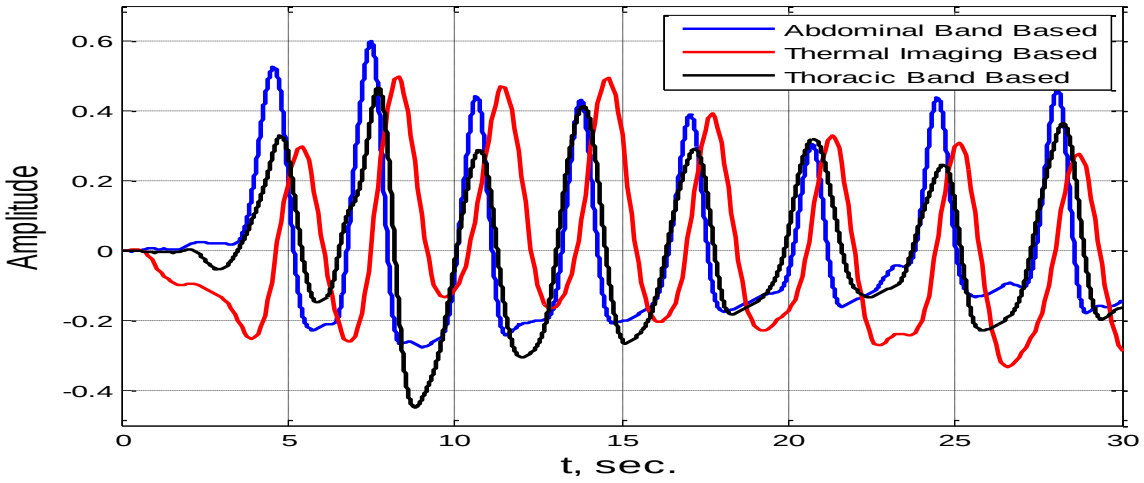

Figure 5 A section of respiration signals obtained using abdominal band, thoracic band and thermal imaging for a subject.

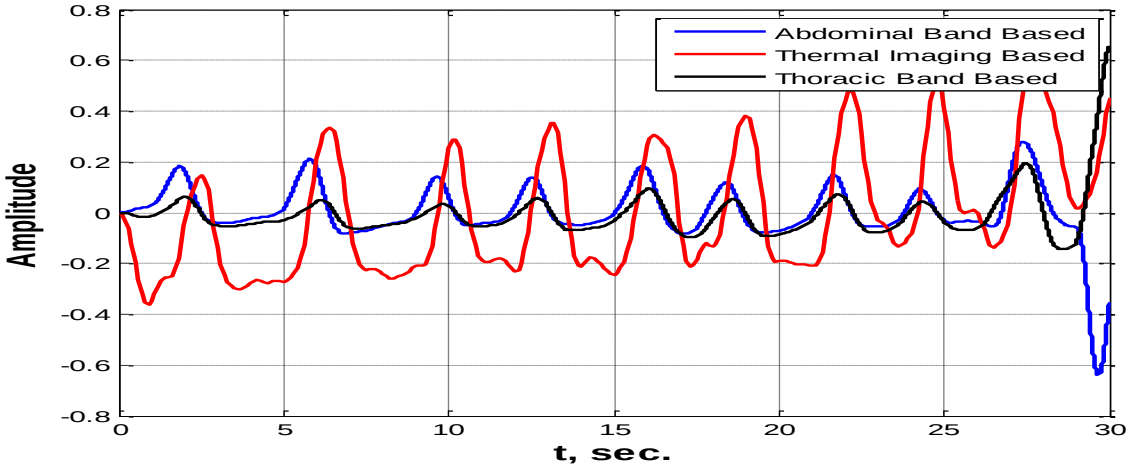

Figure 6 Respiration signals obtained using the abdominal band, thoracic band and thermal imaging for a subject.

The respiration signals obtained using the thermal imaging based method lagged the other two methods, but the amount of the lag was larger for the abdominal band signal as shown in Figure 7.

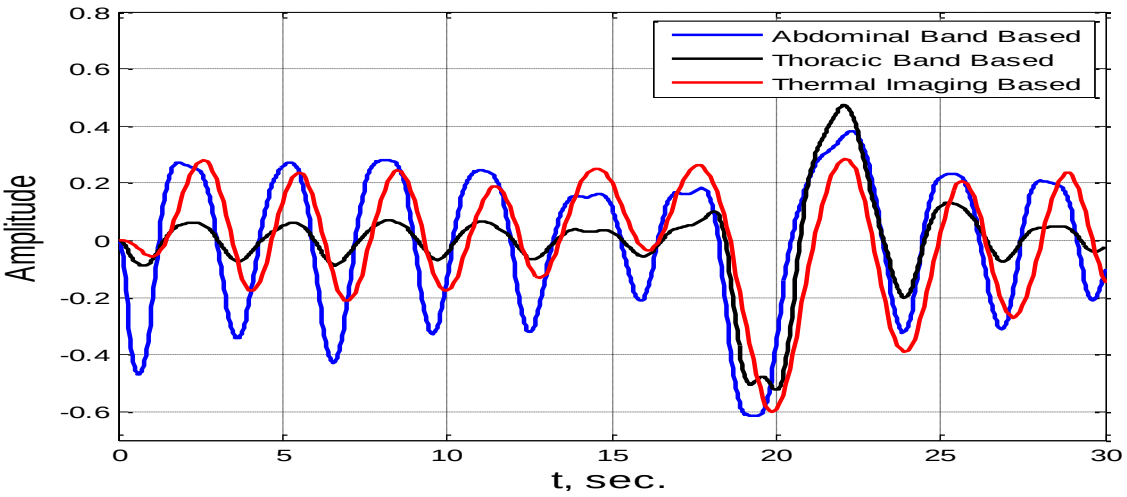

Figure 7 Comparison of respiration signals obtained from abdominal and thoracic bands against thermal imaging based for a subject.

The time delay observed in the thermal imaging based signal is related to the physics of respiration, initiating from exhalation, causing the chest to move back, the

effect then cycling through, warming the skin surface around the nose. The image capture rate difference in the ground truths (capture rate =32 images per second) and the thermal imaging methods (capture rate=10 images per second) may have influenced this effect [41].

Figure 6 shows the respiration signals in which around the 30th second, the abdominal band signal has an opposite phase to those from both the thoracic band and thermal imaging. The thermal imaging signal is in agreement with the thoracic band signal and from the expiratory pause of the previous respiration cycle, it is expected that an inspiration would follow as indicated by both the thoracic band and thermal imaging based signals. The reason for the reversing of the abdominal band signal could be a body movement at the region where the abdominal band had been attached. The thoracic band signal also lagged the abdominal band signal during inspiration and led it during expiration, but the time interval was shorter as seen in Figures 6 and 7.

The differences between the abdominal and thoracic bands respiration signals could be due to the mechanics of breathing. As the diaphragm flattens to initiate inspiration, the effect is mostly registered on the abdominal band. When the diaphragm recoils during expiration, the thoracic band experiences a delayed contraction as compared with the abdominal band.

The respiration rate values for the 15 subjects included in the study are included in Tables 2 and 3.

Table 2 Respiration rates determined using the three methods for 12 of the 15 recorded subjects that did not have large head movements

Subject	Gender	Age (years)	Respiration rate (cycles per minute)		
			Thermal Imaging	Thoracic band	Abdominal band
1	Female	42	11.3	11.3	11.3
2	Male	27	17.4	16.8	16.8
3	Male	32	16.5	16.0	16.0
4	Female	25	22.3	22.5	22.5
5	Female	30	14.1	14.2	14.2
6	Male	36	23.4	22.8	22.8
7	Male	27	19.5	19.7	19.7
8	Female	45	22.0	22.0	22.3
9	Male	55	10.2	11.0	11.0
10	Male	29	15.0	15.0	15.0
11	Male	52	26.0	26.3	26.3
12	Male	22	13.0	13.1	13.1
statistics: mean(m), standard deviation (s), correlation coefficient between thermal imaging and thoracic band (c)	8 males 4 females	m=35.2 s= 10.9	m=17.6 s= 5.1 c=0.997	m=17.6 s=5.0	m=17.6 s=5.1

Table 3 Respiration rates determined using the three methods for 3 of 15 recorded subjects with very large head movements

Subject	Gender	Age (years)	Respiration rate (cycles per minute)		
			Thermal Imaging	Thoracic band	Abdominal band
13	Male	41	20.8	25.9	25.9
14	Male	45	9.4	17.8	17.8
15	Female	27	19.3	20.6	20.6
statistics: mean(m), standard deviation (s)	2 males 1 females	m=37.7 s=9.5	m=16.5 s= 6.2	m=21.4 s=4.1	m=21.4 s=4.1

For the subjects included in Table 2, the mean (17.6 cycles per minute) and standard deviation (5.1 cycle per minute) of their respiration rates as measured by thermal imaging are close to those measured by the abdominal and theoretic bands. The correlation coefficients between the respiration rates values obtained by thermal imaging and those obtained using thoracic and abdominal bands is 0.997.

In subjects 13 to 15, there were very large head movements causing the inner corner of an eye not to be within the camera's field of view. This led to a false detection of

the eye’s corner, an inaccurate detection of the respiration region of interest, incorrect measurement of respiration signal and respiration rate.

The thermal imaging method operated well in situations where the head movements did not cause the face to move out of the camera's field of view and the subject breathed through the nose. Further developments will include incorporating a method to will also cater breathing through the mouth and tacking very large movements by for example automatically rejecting the associated images. A general purpose thermal camera was used in this study. A further area of improvement will be to develop a more customised thermal imaging device for respiration rate monitoring thus reducing the cost and making its use easier.

4 Conclusions

A real-time thermal imaging based noncontact respiration rate monitoring method was developed. Its ability to segment the face from the image background was tested on 55000 images recorded from 14 adults. It extracted the face correctly in all images, but in 11.7% of the images, a section the neck was also included, but this did not affect the accuracy of determining respiration rate values.

The thermal imaging respiration rate monitoring was evaluated on a further 15 adults by comparing it against the contact respiration rate monitoring methods that used thoracic and abdominal bands. In 12 subjects, the respiration rate values obtained using the 3 methods were very close. In the remaining 3 subjects that had very large head movements that led to in a significant proportion of the face to move out of camera's field of view, the respiration rates from the thermal imaging method was not accurate. The existing method works well in scenarios that head movements are not so large to cause the face to move out of camera's field of view.

5 Acknowledgments

The authors are grateful to all subjects who participated in the data recordings. They appreciate the valuable help and support of staff, in particular Dr Ruth Kingshott, at the Sleep Unit of Sheffield Children's Hospital National Health Service Trust, Sheffield, UK.

References

[1] McLafferty, E., Johnstone, C., Hendry, C. and Farley, A.: 'Respiratory system part 1: pulmonary ventilation', Nurs. Stand., 2013, 27, (22), pp. 40-47.

[2] Subbe, C.P., Davies, R.G., Williams, E., Rutherford, P. and Gemmell, L.: 'Effect of introducing the modified early warning score on clinical outcomes, cardio-pulmonary arrests and intensive care utilisation in acute medical admissions', Anaesthesia, 2003, 58, (8), pp.797-802.

[3] Ambrogio, C. and Parthasarathy, S.: 'Polysomnography during critical illness', Journal of Clinical Sleep Medicine, 2007, 3, (6), pp.649-650.

[4] Parthasarathy, S. and Tobin, M.J.: 'Sleep in the intensive care unit', Intensive Care Med., 2004, 30, (2), pp.197-206.

[5] Sampol, G., Romero, O., Salas, A., Tovar, J.L., Lloberes, P., Sagalés, T. and Evangelista, A.: 'Obstructive sleep apnea and thoracic aorta dissection', American Journal of Respiratory and Critical Care Medicine, 2003, 168, (12), pp.1528-1531.

[6] Alkali, A.H., Saatchi, R., Elphick, H. and Burke, D.: 'Facial tracking in thermal images for real-time noncontact respiration rate monitoring', 2013 European Modelling Symposium, 2013, pp. 265-270.

[7] AL-Khalidi, F.Q., Saatchi, R., Burke, D., Elphick, H. and Tan, S.: 'Respiration rate monitoring methods: A review', Pediatr. Pulmonol., 2011, 46, (6), pp. 523-529.

[8] Bartula, M., Tigges, T. and Muehlsteff, J.: 'Camera-based system for contactless monitoring of respiration', Conf Proc. IEEE Engineering in Medicine and Biology Society, 2013, pp. 2672-2675.

[9] Greneker, E.F.: 'Radar sensing of heartbeat and respiration at a distance with applications of the technology', Radar 97 (Conf. Publ. no. 449), 1997, pp.150-154.

[10] Min, S.D., Yoon, D.J., Yoon, S.W., Yun, Y.H. and Lee, M.: "A study on a non-contacting respiration signal monitoring system using Doppler ultrasound', Med. Biol. Eng. Comput., 2007, 45 (11), pp.1113-1119.

[11] Min, S.D., Kim, J.K., Shin, H.S., Yun, Y.H., Lee, C.K. and Lee, M.:, 'Noncontact respiration rate measurement system using an ultrasonic proximity sensor Sensors Journal, IEEE, 2010, 10, pp. 1732-1739.

[12] Nakai, H., Ishihara, K., Miyake, Y. and Watanabe, M.: 'Non-restrictive visual respiration monitoring', IEEEXplore, 2000, pp. 647-651, http://ieeexplore.ieee.org/stamp/stamp.jsp?tp=&arnumber=903001, last accessed 02/11/2015.

[13] Aoki, H., Takemura, Y., Mimura, K., and Nakajima, M.: 'Development of non-restrictive sensing system for sleeping person using fiber grating vision sensor', 2001 International symposium on Micromechatronics and Human Science, 2001, pp.155-160.

[14] Tan, K.S., Saatchi, R., Elphick, H. and Burke, D.: 'Real-time vision based respiration monitoring system', 2010 International Symposium On Communication Systems Networks and Digital Signal Processing, 2010, pp.770-774.

[15] Poh, M.Z., McDuff, D.J. and Picard, R.W.: 'Advancements in noncontact, multiparameter physiological measurements Using a webcam', IEEE Transactions On Biomedical Engineering, 2011, 58, (1), pp.7-11.

[16] Scully, C.G., Lee, J., Meyer, J. Gorbach, A.M., Granquist-Fraser, D., Mendelson, Y. and Chon, K.H.: 'Physiological parameter monitoring from optical recordings with a mobile phone", EEE Transactions On Biomedical Engineering, 2012, 59, (2), pp. 303-306.

[17] Alkali, A.H., Saatchi, R., Elphick, H., Burke, D. and Evans, R.: 'Noncontact respiration rate monitoring based on sensing exhaled air', Malaysian Journal of Fundamental and Applied Sciences, 2013, 9, (3), pp.129-133.

[18] Jones, B.F. and Plassmann, P.: 'Digital infrared thermal imaging of human skin', IEEE Engineering in Medicine and Biology, 2002, 21, pp. 41-48.

[19] Yang, G. and Huang, T.S.: 'Human face detection in a complex background', Pattern Recognition, 1994, 27,(1), pp.53-63.

[20] Yang, M.H., Kriegman, D., and Ahuja, N.: 'Detecting faces in images: a survey', IEEE Transactions On Pattern Analysis and Machine Intelligence, 2002, 24,(1), pp. 34-58.

[21] Mostafa, E., Farag, A., Shalaby, A., Ali, A., Gault, T. and Mahmoud, A.: 'Long term facial parts tracking in thermal imaging for uncooperative emotion recognition', IEEEXplore, 2013, http://ieeexplore.ieee.org/stamp/stamp.jsp?arnumber=6712739, last accessed 26/10/2015

[22] Viola, P. and Jones, M.: 'Rapid object detection using a boosted cascade of simple features', Proceedings of Conference on Computer and Pattern Recognition,

2001, https://www.cs.cmu.edu/~efros/courses/LBMV07/Papers/viola-cvpr-01.pdf, last accessed 26/10/2015.

[23] Lienhart, R. and Maydt, J.: 'An extended set of Haar-like features for rapid object detection',2002, http://www.lienhart.de/Prof._Dr._Rainer_Lienhart/Source_Code_files/ICIP2002.pdf, last accessed 26/10/2015.

[24] Hanawa, D., Morimoto, T., Shimazaki, S., Oguchi, K, Tsuchiya, R. Mochiduki, K. Furusato, M. and Oguchi K.: 'Nasal cavity detection in facial thermal image for non-contact measurement of breathing', International Journal of Advances in Telecommunications, Electrotechnics, Signals and Systems, 2013, 2, (1), pp. 33-38.

[25] AL-Khalidi, F.Q., Saatchi, R. Burke, D. and Elphick, H.: 'Tracking human face features in thermal images for respiration monitoring', 2010 IEEE/ACS International Conference On Computer Systems and Applications, 2010, pp. 1-6.

[26] Martinez, B., Binefa, X., and Pantic, M.: 'Facial component detection in thermal imagery', 2010 IEEE Computer Society Conference On Computer Vision and Pattern Recognition, 2010, pp. 48-54.

[27] Fei, J., Zhu, Z. and Pavlidis, I.: 'Imaging breathing rate in the CO2 Absorption band', Proceedings of 2005 IEEE in Engineering in Medicine and Biology 27th Annual Conference, 2005, pp. 700-705.

[28] Lucas, D. and Kanade, T.: 'An iterative image registration technique with an application to stereo vision', Proceedings of 7th International Joint Conference on Artificial Intelligence, 1981, pp. 674-679, https://www.ces.clemson.edu/~stb/klt/lucas_bruce_d_1981_1.pdf, last accessed 26/10/2016.

[29] Fei, J. and Pavlidis, I., 'Thermistor at a distance: unobtrusive measurement of breathing', IEEE Transactions On Biomedical Engineering, 2010, 57, (4), pp. 988-998.

[30] Murthy, J.N., van Jaarsveld, J., Fei, J., Pavlidis, I., Harrykissoon, R.I., Lucke, J.F., Faiz, S. and Castriotta, R.J.: 'Thermal infraed imaging: a novel method to monitor airflow during polysomnography', Sleep, 2009, 32, (11), pp. 1521-1527.

[31] Dowdall, J., Pavlidis, I.T. and Tsiamyrtzis, P.: Colitional tracking, Computer Vision and Image Understanding, Elsevier, 2007, 106, pp. 205-219.

[32] Shastri, D. and Pavlidis, I.: 'Automatic initiation of the periorbital signal extraction in thermal imagery', 2009, Advanced Video and signal Based Surveillance, IEEE Computer Society, IEE Explore, pp.182- 186. http://ieeexplore.ieee.org/stamp/stamp.jsp?tp=&arnumber=5280058, last accessed 12/04/2016.

[33] Zhou, Y., Tsiamyrtzis, P., Lindner, P., Timofeyev, I. and Pavlidis, I.: 'Spatiotemporal smoothing as a basis for facial tissue tracking in thermal imaging', IEEE Transaction on Biomedical Engineering, 2013, 60, (5), pp. 1280-1289.

[34] Edelman, G.J., Hoveling, R.J., Roos, M., van Leeuwen, T.G., and Aalders, M.C.: 'Infrared imaging of the crime scene: possibilities and pitfalls', J. Forensic Sci., 2013, 58, (5), pp.1156-1162.

[35] Memarian, N., Chau, T. and Venetsanopoulos, A.N.: 'Application of infrared thermal imaging in rehabilitation engineering: preliminary results', 2009 IEEE Toronto International Conference in Science and Technology for Humanity, 2009, pp.1-5.

[36] Otsu, N.: 'A Threshold selection method from gray-level histograms', IEEE Transactions On Systems, Man and Cybernetics, 1979, 9, (1), pp. 62-66.

[37] Tsai, W.: 'Moment-preserving thresolding: a new approach', Computer Vision, Graphics, and Image Processing, 1985, 29, pp.377-393, https://ir.nctu.edu.tw/bitstream/11536/4803/1/A1985ADW8000009.pdf, last accessed 26/10/2015.

[38] Kapur, J.N., Sahoo, P.K., and Wong, A.K.C.: 'A new method for gray-level picture thresholding using the entropy of the histogram', Computer Vision, Graphics, and Image Processing, 1985, 29, (3), pp. 273-285.

[39] Young, J.W.: 'Head and face anthropometry of adult U.S. citizens', Office of Aviation Medicine, Washington D.C. 20591, 1993, http://www.faa.gov/data_research/research/med_humanfacs/oamtechreports/1990s/media/am93-10.pdf, last accessed 26/10/2015.

[40] Farkas, L.G., Katic, M.J., Forrest, C.R., Alt, K.W., Bagic, I., Baltadjiev, G., Cunha, E., Cvicelová, M., Davies, S., Erasmus, I., Gillett-Netting, R., Hajnis, K., Kemkes-Grottenthaler, A., Khomyakova, I., Kumi, A., Kgamphe, J.S., Kayo-daigo, N. , Le, T., Malinowski, A., Negasheva, M., Manolis, S., Ogetürk, M., Parvizrad, R., Rösing, F., Sahu, P., Sforza, C., Sivkov, S., Sultanova, N., Tomazo-Ravnik, T., Tóth, G., Uzun, A., Yahia, E.: 'International anthropometric study of facial morphology in various ethnic groups/races', Journal of Craniofacial Surgery, 2005, 16, (4), pp. 615-646.

[41] Murthy, R., Pavlidis, I. and Tsiamyrtzis, P.: 'Touchless monitoring of breathing function', 26th Annual International Conference of the IEEE in Engineering in Medicine and Biology Society, 2004, 2, pp. 1196-1199.